A Suzaku Observation of the Neutral Fe-line Emission from RCW 86

Masaru UENO,[1] Rie SATO,[1] Jun KATAOKA, [1] Aya BAMBA,[2] Ilana HARRUS, [3,4]
Junko HIRAGA,[2] John P. HUGHES,[5] Caroline A. KILBOURNE, [4] Katsuji KOYAMA, [6]
Motohide KOKUBUN,[7] Hiroshi NAKAJIMA, [6] Masanobu OZAKI,[8] Robert PETRE,[4]
Tadayuki TAKAHASHI,[8] Takaaki TANAKA,[8] Hiroshi TOMIDA,[9] and Hiroya YAMAGUCHI [6]

[1] *Department of Physics, Faculty of Science, Tokyo Institute of Technology, 2-12-1, Meguro-ku, Ohokayama, Tokyo 152-8551, Japan*
E-mail(MU): masaru@hp.phys.titech.ac.jp

[2] *RIKEN (The Institute for Physics and Chemical Research) 2-1, Hirosawa, Wako-shi, Saitama, Japan*

[3] *Department of Physics and Astronomy, Johns Hopkins University, Baltimore, MD, 21218, USA*

[4] *NASA Goddard Space Flight Center, Laboratory for High Energy Astrophysics, Code 662, Greenbelt, MD 20771, USA*

[5] *Department of Physics and Astronomy, Rutgers University 136 Frelinghuysen Road, Piscataway, NJ 08854-8109, USA*

[6] *Department of Physics, Graduate School of Science, Kyoto University, Sakyo-ku, Kyoto 606-8502, Japan*

[7] *Department of Physics, University of Tokyo, 7-3-1 Hongo, Bunkyo-ku, Tokyo, Japan*

[8] *Institute of Space and Astronautical Science, Japan Aerospace Exploration Agency 3-1-1 Yoshinodai, Sagamihara, Kanagawa 229-8510, Japan*

[9] *ISS Science Project Team, Institute of Space and Astronautical Science, Japan Aerospace Exploration Agency 2-1-1, Sengen, Tsukuba, Ibaraki 305-8505, Japan*

(Received ; accepted)

Abstract

The newly operational X-ray satellite Suzaku observed the supernova remnant (SNR) RCW 86 in February 2006 to study the nature of the 6.4 keV emission line first detected with the Advanced Satellite for Cosmology and Astronomy (ASCA). The new data confirms the existence of the line, localizing it for the first time inside a low temperature emission region and not at the locus of the continuum hard X-ray emission. We also report the first detection of a 7.1 keV line that we interpret as the Kβ emission from neutral or low-ionized iron. The Fe-K line features are consistent with a non-equilibrium plasma of Fe-rich ejecta with $n_e t \lesssim 10^9$ cm^{-3} s and $kT_e > 1$ keV. We found a sign that Fe Kα line is intrinsically broadened 47 (35–57) eV (99% error region). Cr-K line is also marginally detected, which is supporting the ejecta origin for the Fe-K line. By showing that the hard continuum above 3 keV has different spatial distribution from the Fe-K line, we confirmed it to be synchrotron X-ray emission.

Key words: ISM:individual (RCW 86) – supernova remnants – X-rays:ISM

1. Introduction

Since synchrotron X-ray emission was for the first time localized to a shell of a supernova remnant, SN1006 (Koyama et al. 1995), a number of young SNRs have been proven to show synchrotron X-rays from their shells [see for example, Cas A (Hughes et al. 2000); Tycho (Hwang et al. 2002); or G347.3−0.5 (Slane et al. 2001)]. Synchrotron X-ray emission is from electrons with energies up to 10 TeV and therefore, is the strongest evidence to date of particle acceleration in the diffuse shocks of young SNRs.

RCW 86 is one of the SNRs from which hard X-ray emission, which can be synchrotron emission, has been discovered. It has, however, a distinct characteristic to have hard X-ray emission from a south-west part of the remnant associated with a neutral Fe-K line emission. Since the line is discovered in 1997 in the ASCA observations of the remnant (Vink et al. 1997), its origin remains a mystery and the origin of the hard X-ray emission has also been unknown: synchrotron or another mechanism. In the initial paper, Vink et al. (1997) tried to explain peculiar combination of abundances, the strong 6.4 keV-line and weak line emission of light elements, by an electron distribution with a supra-thermal tail. BeppoSAX observations confirmed the existence of 6.4 keV line from the south-west region of RCW 86 (Bocchino et al. 2000). They found spatial variation of hardness in the SW region, and explained the peculiar abundances by mixture of two-temperature plasmas: low abundance low-temperature and high abundance high-temperature plasmas. They attributed the latter plasma to Fe-rich ejecta. The detection of high-energy (> 10 keV) emission by RXTE (Petre et al. 1999) suggested the existence of non-thermal X-ray emission. Bamba et al. (2000) and Borkowski et al. (2001a) found that the ASCA spectrum from the SW region can be explained by a combination of three components: low and high temperature plasmas, and non-thermal (synchrotron) emission. Using the superior high spatial resolution of Chandra, Rho et al. (2002) spatially resolved the low-temperature plasma and the hard continuum emission. By showing spatial correlation between the

hard continuum and radio emission, they confirmed that the hard continuum originates from synchrotron emission. Since they found the Fe Kα line only from the region of the hard continuum, they suggested that the synchrotron X-ray is emitted from Fe-rich ejecta. Hard X-ray emission from a north-east region of RCW 86 shows no evidence for a 6.4 keV line, and Vink et al. (2006) recently reported discussions on the ground that the origin of that emission is synchrotron.

Since spatial distribution of the 6.4 keV-line and precise spectroscopy of the line features will give us important information on the emission mechanism of the line, we performed a Suzaku observation on the south-west part of RCW 86. In this paper, we mainly report on the results in the hard band (> 3 keV); hard continuum, and Fe-line features. We assume a kinematic distance of 3 kpc (Rosado et al. 1996).

2. SUZAKU Observation of RCW 86

Suzaku is a joined Japanese-US mission that was launched in July 2005 (Mitsuda et al. 2006). Two instruments, the XIS and HXD, are operational. The XIS consists of 4 independent CCDs cameras, three front-illuminated (energy range 0.4–12 keV) and one back-illuminated (energy range 0.2–12 keV). Each is located in the focal plane of a dedicated nested thin-foil X-ray telescope (XRTs). The total effective area is quite large ($\sim$ 1000 cm^{-2} at 6 keV). In addition, the low-Earth orbit of Suzaku contributes to a low and reproducible background. The HXD is a non-imaging collimated detector which extends the bandpass of the observatory up to 600 keV. More information on the mission and the instruments on board (XRT, XIS, and HXD) can be found in Serlemitsos et al. (2006), Koyama et al. (2006), and Takahashi et al. (2006).

The south-west region of RCW 86 was observed by Suzaku in February 2006. At the writing of this paper, the background determination for the HXD is still not complete and we chose not to include any HXD data in our analysis. The XIS contamination (Koyama et al. 2006) plays no role at the energies of the Fe-K line, our main concern for this paper.

The data (revision 0.7; Mitsuda et al. 2006) were analyzed after the following filtering. Data taken with low data rate, at low elevation angle from the Earth rim ($<5°$), or during passage through the South Atlantic Anomaly were removed. We also removed data from hot and flickering pixels using the `cleansis` software. In order to suppress the hard-band background of XIS 1, which is higher than that of XIS 0, 2, or 3, data taken at low cut-off rigidity regions (< 6 GV) were also removed from the XIS 1 data additionally. The resultant exposure times are 116 ks for each XIS 0, 2, 3 and 96 ks for XIS 1. At this stage of the mission, the attitude is not completely correct and we used a point source detected in an XMM-Newton observation of RCW 86, to correct the absolute coordinate system of our observation. The correction is rather small (ΔRA=$-0.^\circ0044$, ΔDec=$-0.^\circ0049$) for all 4 of the XIS.

3. XIS Images

Figures 1a and b show XIS intensity contours in the low (0.5–1.0 keV) and high (3.0–6.0 keV) energy bands. The high-energy band was chosen to show the contribution from the continuum only. We have shown on Fig. 1a, the 6.4 keV-line intensity image. This image was generated by subtracting from the (6.34–6.46 keV) image, the continuum contribution extracted from the (5.0–6.2 keV) image. Relative normalization between these images is done using a power-law model. Since smoothing may show artificial structures, we adaptively binned the image using the weighted Voronoi tessellation algorithm implemented by Diehl & Statler (2006), which is based on the algorithm of Cappellari & Copin (2003). The size of each bin was determined so that significance of the 6.4 keV line is at least 5σ. The resulting image is shown in Fig. 1b. In order to quantify spatial correlation between the 6.4 keV line and the continuum emission, we furthermore obtained spatial variation of count-rate ratios between the 6.4 keV line and the (5.0–6.2 keV) band using the same binning. The result is shown in Fig. 2 with the 3.0–6.0 keV intensity contours. If we multiply the ratio by 3, it corresponds to the equivalent width (keV) of the 6.4 keV line at that position. We have generated in Fig. 3 a true color image of the remnant showing the spatial variations between low and high-energy continuum (shown in blue and red respectively), and the region of emission of the 6.4 keV-line (shown in green).

The spatial distribution of the 6.4 keV-line is revealed for the first time thanks to combination of the large effective area and the low-background of Suzaku at the energy band around 6.4 keV. The red region in Fig. 3 corresponds to the location of the low-temperature plasma, which was attributed to the forward shock by Rho et al. (2002), whereas the blue region corresponds to the filamentary structures of the hard X-ray emission revealed by the Chandra observation (Rho et al. 2002). The 6.4 keV-line is emitted from the inner part of the red region, or the forward shock. As apparent in Fig 1b, the high-energy continuum emission from the remnant does not correlate with the position of the maximum intensity of the 6.4 keV-line. Fig. 2 shows that the equivalent width of the 6.4 keV line and the continuum emission rather anti-correlate with each other, the origins of the line and the continuum are strongly suggested to be different. We will examine below how the spectral analysis of the line fit with this new finding.

4. Spectral Analysis of the 6.4 keV Line

In order to study the origin of the 6.4 keV emission line, we extracted spectra from a region shown in Fig. 1, an elliptical region of $12'.5 \times 9'.2$ diameters with its center on (RA, DEC)$_{J2000}$ = ($14^h41^m08^s.7$,$-62^\circ40'10''$) inclined for 20°. This region was chosen so that maximum signal-to-noise ratio can be obtained for the 6.4 keV line. Even though one may expect three distinct spectra from three color regions in Fig. 2, the spatial resolution of XIS did

Table 1. Suzaku Observations Appearing in this Paper.

Target	Observation ID	Date	Exposure[a] (ks)
RCW 86 Southwest	500004010	2006/02/12–14	116.5/96.4
North Ecliptic Polar	500026010	2006/02/10–12	96.0/87.5
High Latitude A	500027010	2006/02/14–15	79.5/71.1
Sgr C	500018010	2006/02/20–23	114.5/98.6

[a] Exposure times for *XIS0,2,3/XIS1* after the data screening.

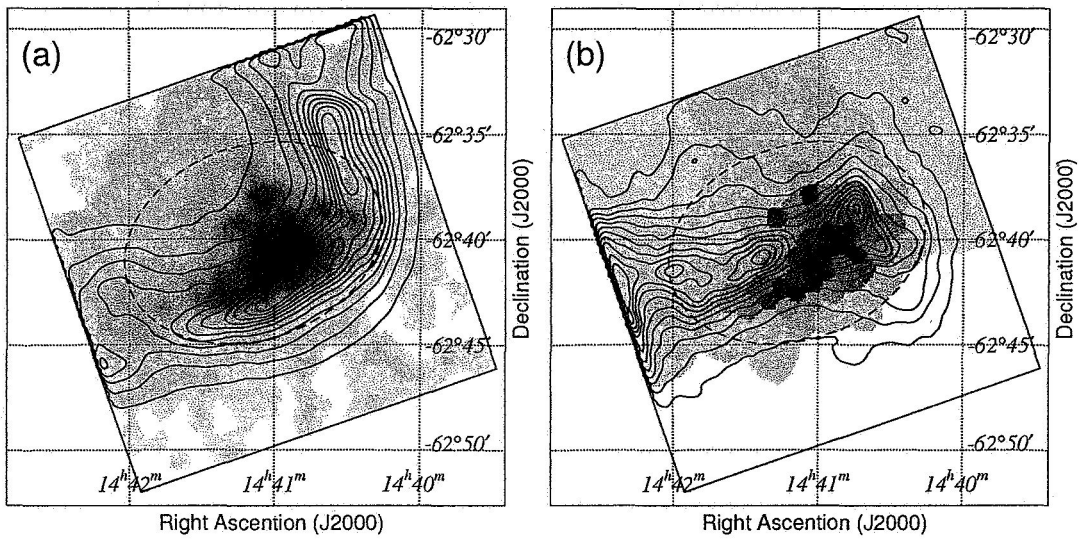

Fig. 1. XIS 0.5–1.0 keV (a) and 3.0–6.0 keV (b) intensity contours overlaid by the 6.4 keV-line images. The 6.4 keV line image in (a) is smoothed with a Gaussian kernel of σ=25″, whereas that in (b) is adaptively binned using the weighted Voronoi tessellation algorithm (Diehl & Statler 2006). Images and contours are in linear scale. The spectral region is shown with a broken-line ellipse. The XIS field of view is designated with a solid-line square in each image.

not allow us such distinct separation. Moreover Chandra and XMM-Newton are better in spatially resolved spectroscopy for the soft component and the hard continuum emission. Therefore we here concentrate on the spectroscopy of the Fe-K line features.

As the entire field of view is covered by the remnant, we used "blank-sky" observations, extracting the background from the same regions on the detectors as the ones used in the analysis. Both observations ("North Ecliptic Polar" and "High Latitude A", see Table 1) were carried out either immediately before or after our observation of RCW 86, insuring an identical response of the detector. Spectra of these two observations were weighted averaged using the exposure time. Above 3 keV, differences between the responses from all the FI chips are negligible and we summed the spectra of XIS 0, 2 and 3 for the following analysis. Although the BI is kept and analyzed separately, the differences between the summed FI and the BI-derived spectral parameters are negligible.

Background-subtracted spectra in the energy band 3.0–10 keV are shown in Fig. 4. Since we see power-law like spectrum with two conspicuous lines at 6.4 and 7.1 keV, we fitted the spectrum with a power-law function plus two Gaussians corrected for the interstellar absorption. Since absorption column is not well determined by those hard band spectra, we fixed the column density $N_{\rm H}$ to 5×10^{21} cm^{-2}, which is close to the values obtained by Rho et al. (2002) for the SW regions. Note that following results have no strong dependence on the column density. The standard RMF files version 2006-02-13 were used, whereas ARF files were produced by the `xissimarfgen` software version 2006-05-28 with CALDB version 2006-05-24 assuming uniform emission from the spectral region. As a result, we obtained an acceptable fit (χ^2/degree of freedom (dof) = 270.7/291) with the best-fit parameters given in Table 2. The best-fit model is shown in Figure 4. Note that there is a systematic error of about 15 eV in the center energy of the lines. The 7.1 keV line is detected clearly for the first time.

Although the model is reproducing the overall spectrum quite well, we still see some data excess against the best-fit model at ~5.4 keV in Fig. 4. When we added a Gaussian with a fixed σ (40 eV) to the model, the fit was improved with χ^2/dof = 258.5/289. The best-fit center energy and the flux of the Gaussian were 5.38 (5.32–5.43) keV and 2.7 (1.5–3.9)$\times 10^{-6}$ photons cm^{-2} s^{-1}, respectively. If we apply the F-test, the significance level of this additional Gaussian is ~ 99.9%. The center energy is consistent with

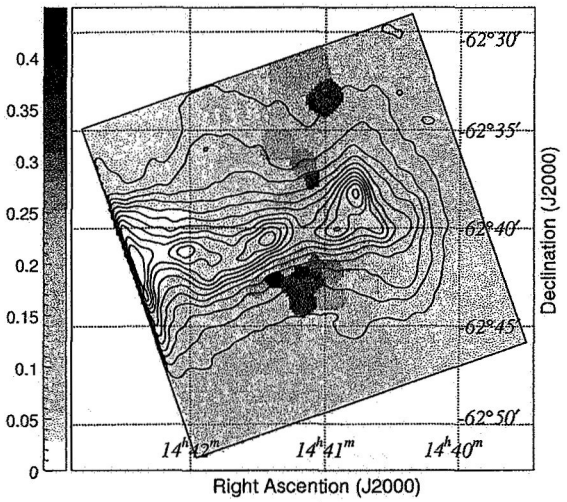

Fig. 2. Count-rate ratio map between the 6.4 keV line and the 5.0–6.2 keV band overlaid with contours of the 3.0–6.0 keV intensity map. By multiplying 3, a ratio can be converted to an equivalent width (keV) of the 6.4 keV line at that position.

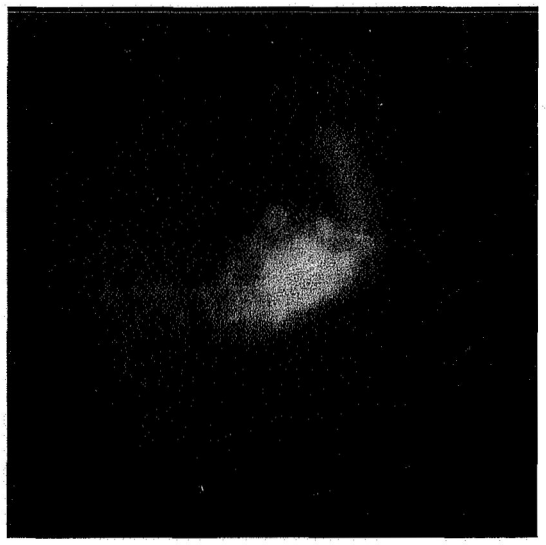

Fig. 3. True color XIS image of the RCW 86 south-west region: red represents 0.5–1.0 keV photons; blue represents 3.0–6.0 keV photons; and green represents 6.4 keV emission.

the Kα-line energy of neutral chromium (5.41 keV).

Since existence of neutral iron at the SW region is suggested by the Fe-K emission lines, and it may cause absorption, we further tried adding Fe K-edge to the model with the energy fixed to the center energy of the 6.4 keV line plus 0.712 keV. As a result, the fit was slightly improved (χ^2/dof = 255.6/288) with the iron column density $N_{\rm Fe} = 1.7\ (0.88\text{–}3.5) \times 10^{18}$ cm^{-2}. If we apply the F-test, the significance level of existence of Fe K-edge is $\sim$ 93%.

In order to distinguish between instrumental and intrinsic width, we compared them with those derived from an

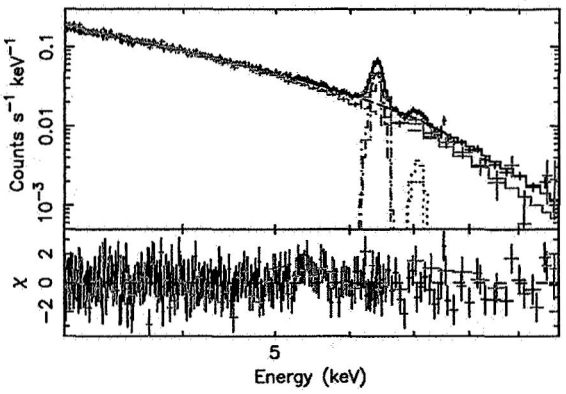

Fig. 4. Background-subtracted spectra in the hard energy band (>3 keV). Data points of XIS 0+2+3 and XIS 1 are shown with black and red crosses, respectively. Solid-lines show the best-fit model of a power-law function plus two Gaussians.

Table 2. Best-fit parameters of the hard X-ray emission with a power-law function plus two Gaussians.

Parameters	Values
Power-law	
Γ	3.17 (3.14–3.19)
norm[a]	3.5 (3.3–3.6)
6.4 keV-line	
Center (keV)	6.404 (6.400–6.407)
σ[b] (eV)	61 (56–66)
Flux[c]	5.1 (4.9–5.3)
7.1 keV-line	
Center (keV)	7.08 (7.04–7.11)
σ[b] (eV).....	69 (35–101)
Flux[c].....	0.53 (0.40–0.69)
$N_{\rm H}$ (cm^{-2}) ...	5×10^{21} (fixed)
χ^2/dof	270.7/291

Notes. Error regions correspond to 90% confidence levels.
[a] Normalization at 1 keV ($\times 10^{-2}$ photons keV^{-1} cm^{-2} s^{-1}).
[b] This value includes detector energy resolution (see text).
[c] Total flux ($\times 10^{-5}$ photons cm^{-2} s^{-1}) in the line.

identical analysis done on the Sgr C observation (Table 1) which was performed 8 days after the RCW 86 observation. The 1σ width of 6.4 keV in the Sgr C observation was 39 (34–44) eV. Since the 6.4 keV line from Sgr C, a molecular cloud, is expected to have negligible intrinsic width compared with the energy resolution of XIS, the width is thought to be instrumental energy resolution Therefore, the difference of the 6.4 keV line widths between these two observations should show the intrinsic width of the 6.4 keV line from RCW 86, which can be calculated to be 47 (35–57) eV (99% error region).

5. Discussion

The location of the 6.4 keV line has been revealed for the first time by the Suzaku observation, and shows that the line and the continuum emissions have different origin, even though both of them are located at the inner part of the shell and are likely to come from ejecta. The solar abundance of chromium relative to iron is ~ 0.01 (Anders & Grevesse 1989) and if both of Fe and Cr K-α lines are excited by electrons (see following discussions), the relative strength of these lines should be ~ 0.01. However, the observed strength of the Cr Kα line is 0.05 (>0.03; 99% region) times that of Fe Kα line. It suggests that the abundance of chromium was enriched by a supernova explosion, especially that of Type Ia (Iwamoto 1999). Therefore, the marginal detection of a Cr-K line also supports the ejecta origin of the Fe-K line.

The Fe-K line features may be fluorescence caused by irradiation. Irradiation in this case is the continuum hard X-ray emission. We estimate required amount of iron by assuming a simple geometry in which the irradiation source is a point-like and iron surrounding it is spherically symmetrical. Then, the required column density of iron $N_{\rm Fe}$ to explain the equivalent width ($\sim$ 500 eV) of the 6.4 keV line is $\sim 8 \times 10^{19}$ cm^{-2}. If we assume 4.4 pc (5′ at 3 kpc) for the radius of the sphere, the mass of iron is 5.8×10^{36} g or $\sim$3000 M$_\odot$. This is too large for ejecta. If we assume solar abundance, the column density of iron corresponds to a column density of interstellar medium $N_{\rm H} \sim 2 \times 10^{24}$ cm^{-2}. However, no such large molecular cloud is reported in the SW region. The column density of iron obtained from the Fe K-edge is also discrepant from the required value.

We next discuss the low-ionized plasma scenario for the 6.4 keV line. From the absence of L-shell lines Borkowski et al. (2001a) have pointed out that M-shell electrons have to be still bounded. The Fe K$_\beta$ line, which was detected for the first time with Suzaku/XIS, gives more clear constraint on the ionization state of iron. The intensity ratio between Fe K$_\alpha$ and K$_\beta$ lines, which is calculated to be 0.10 (0.074–0.14) (99% error region), is consistent with neutral iron, and shows that even if iron is ionized the mean charge is at most +12 (e.g., Palmeri et al. 2003; Mendoza et al. 2004). The center energies of the Fe K$_\alpha$ and K$_\beta$ lines are also consistent with this ionization state (e.g., Palmeri et al. 2003; Mendoza et al. 2004). According to Porquet et al. (2001), see their Fig. 19, in plasmas of almost all temperatures found in SNRs (5×10^6–8×10^7 K), iron is ionized to a mean charge of +9–+10 when the ionization parameter $n_e t$ is 10^9 cm^{-3} s. If we interpolate the curves for $n_e t$= 10^9 and 10^{10} cm^{-3} s, the mean charge of +12 corresponds to $\sim 3 \times 10^9$ cm^{-3} s. Therefore, $n_e t$ has to be $\sim 3 \times 10^9$ cm^{-3} s or smaller. If we assume the plasma age is older than 1000 yr, the electron number density n_e in the plasma has to be smaller than 0.1 cm^{-3}.

On the other hand, there is a required size for the emission measure ${\rm EM_{Fe}} = \int n_e n_{\rm Fe} dV$ to explain the strength of Fe K$_\alpha$ line. If we assume a pure iron non-equilibrium plasma (an NEI model; Borkowski et al. 2001b) of kT_e = 1 keV and $n_e t = 1 \times 10^9$ cm^{-3} s, ${\rm EM_{Fe}}$ has to be $1.9 \times 10^{60} d_{3kpc}^2$ cm^{-3}. The elliptical extraction region of 12.′5 × 9.′2 corresponds to 11×8 pc^2 at 3 kpc distance. Assuming a uniform density of a prorate sphere with $11 \times 11 \times 8$ pc^3 diameters, we arrive at $n_e n_{\rm Fe} = 0.006\ d_{3kpc}^{-1}$ cm^{-6}. If we apply the upper limit of the electron density, the density of iron n_{Fe} has to be larger than 0.06 cm^{-3} d_{3kpc}^{-1}. This density corresponds to an iron mass of $\sim 8 \times 10^{34}\ d_{3kpc}^2$ g or $\sim$40 M$_\odot$, which is too large for an ejecta. Therefore, the electron temperature has to be higher than 1 keV. If $kT_e = 2$ keV is assumed, both the required ${\rm EM_{Fe}}$ and iron mass are about 60 times smaller than those in the 1 keV case, and can be acceptable. The equivalent width of the Fe Kα line against the continuum is 530 (480–580) eV. If we assume an NEI plasma of $kT_e = 2$ keV and $n_e t = 1 \times 10^9$ cm^{-3} s, this equivalent width corresponds to an iron abundance of 1.5. Since most of the detected continuum emission is thought to be from a different region from the Fe Kα line, this abundance sets a lower limit. Although the Suzaku observation found new aspects on the Fe-K line features and gave more concrete limits on the physical parameters, the non-equilibrium plasma of Fe-rich ejecta proposed by Bamba et al. (2000) and Borkowski et al. (2001a) is still valid for the Fe-K line origin.

Even though the 6.4 keV line can be explained with a low-ionized plasma of ejecta, this scenario requires rather large mass of iron. Since electrons of $\sim$100 keV energy have the smaller cross section for the outer orbital electrons and the larger cross section for the inner shell electrons than $\sim$ 10 keV electrons, if we assume harder population for electrons, the required $n_e t$ and $n_e n_{\rm Fe}$ become larger and smaller, respectively, and therefore the required amount of iron can be moderated. A non-thermal (suprathermal) spectrum is the hardest case for the electron population. For example, if we assume electrons in a rather hard power-law of index 0.3 with cut-off at 90 keV which are assumed for the galactic ridge emission by Valinia et al. (2000), the required size of $n_e n_{\rm Fe}$ to explain the 6.4 keV line strength is $6 \times 10^{-6}\ d_{3kpc}^{-1}$ cm^{-6}. This is 1000 times smaller than the case of $kT_e = 1$ keV, and therefore the lower limit of iron mass is less than 0.1 M$_\odot$. Since electrons in such hard population would accompany X-ray continuum via bremsstrahlung which is harder than the detected X-ray continuum (a power-law of photon index $\sim$3.2), X-ray analysis of the existing HXD data may detect such hard X-rays, whose spatial correlation to the 6.4 keV line may be shown by future instruments.

If only collisional interaction is taking place between electrons and ions, kinetic temperature of them are not equilibrated with each other at the ionization parameter of $\sim 10^9$ cm^{-3} s (Itoh 1984), and the ion kinetic temperature is expected to be 10 times or more larger than the electron temperature, or $\gtrsim$10 keV. This high temperature suggests a high shock velocity of $\gtrsim$3000 km s^{-1}. This value is discrepant with the blast-wave velocity of $\sim$400–900 km s^{-1} determined from observations of Balmer-dominated shocks (Ghavamian et al. 2001). Plausible

shocks in the inner part of the shell may have higher velocity than the forward shock. The intrinsic width of ~ 47 eV found for the 6.4 keV line may be evidence of this high velocity. The forward shock might have decelerated by colliding with a cavity wall, whereas the inner shock might be remaining inside the cavity, or a reflected shock after the collision may be moving into the inner region. The cavity wall interaction has also been suggested by Vink et al. (1997) to explain the overall morphology of RCW 86.

We revealed that the hard X-ray continuum in the inner part exists separately from the 6.4 keV line, and therefore confirmed it to be synchrotron emission. In order to meet the condition for synchrotron X-ray to be emitted under the standard diffusive shock acceleration (e.g., Drury 1983), the shock velocity has to be larger than ~ 2000 km s^{-1} independent on the magnetic field strength (Aharonian & Atoyan 1999). A high velocity shock in the inner part of the shell is also required to explain the synchrotron X-rays.

An observation with higher energy resolution on the SW region is highly encouraged. More strict constraint on the iron ionization state can be obtained by measuring the difference between center energies of the 6.4 and 7.1 keV lines at several eV resolution (e.g., Palmeri et al. 2003; Mendoza et al. 2004). Intrinsic width of the 6.4 keV line and existence of Cr-K line can also be verified clearly.

6. Summary

With the large effective area and low background of XIS in the hard X-ray band, we obtained following observational results on the hard X-ray continuum and Fe-line features from the SW region of RCW 86.

1. Spatial distribution of the 6.4 keV line is revealed for the first time.
2. Fe Kβ line is detected for the first time.
3. Strength of Fe K-edge is determined.
4. We found a sign that Fe Kα line is intrinsically broadened for about 50 eV.
5. Cr-K line is marginally detected.

All these results are consistent with that the 6.4 keV line is emitted from a low-ionized plasma of Fe-rich ejecta. We revealed that the hard X-ray continuum is located separately from the 6.4 keV line, and therefore confirmed it to be synchrotron emission.

M.U., R.S., H.N., and H.Y. are supported by JSPS Research Fellowship for Young Scientists. JPH acknowledges support by NASA grant No. NNG05GP87G.

References

Aharonian, F. A., & Atoyan, A. M. 1999, A&A, 351, 330
Anders, E., & Grevesse, N. 1989, Geochim. Cosmochim. Acta, 53, 197
Bamba, A., Koyama, K., & Tomida, H. 2000, PASJ, 52, 1157
Bocchino, F., Vink, J., Favata, F., Maggio, A., & Sciortino, S. 2000, A&A, 360, 671
Borkowski, K. J., Rho, J., Reynolds, S. P., & Dyer, K. K. 2001a, ApJ, 550, 334
Borkowski, K. J., Lyerly, W. J., & Reynolds, S. P. 2001b, ApJ, 548, 820
Cappellari, M., & Copin, Y. 2003, MNRAS, 342, 345
Diehl, S., & Statler, T. S. 2006, MNRAS, 368, 497
Drury, L. O. 1983, Reports of Progress in Physics, 46, 973
Ghavamian, P., Raymond, J., Smith, R. C., & Hartigan, P. 2001, ApJ, 547, 995
Hwang, U., Decourchelle, A., Holt, S. S., & Petre, R. 2002, ApJ, 581, 1101
Hughes, J. P., Rakowski, C. E., Burrows, D. N., & Slane, P. O. 2000, ApJL, 528, L109
Itoh, H. 1984, ApJ, 285, 601
Iwamoto, K., Brachwitz, F., Nomoto, K., Kishimoto, N., Umeda, H., Hix, W. R., & Thielemann, F.-K. 1999, ApJS, 125, 439
Kaastra, J. S., & Mewe, R. 1993, A&AS, 97, 443
Koyama, K., Petre, R., Gotthelf, E. V., Hwang, U., Matsuura, M., Ozaki, M., & Holt, S. S. 1995, Nature, 378, 255
Koyama, K., et al. 2006, PASJ, this volume
Mendoza, C., Kallman, T. R., Bautista, M. A., & Palmeri, P. 2004, A&A, 414, 377
Mitsuda, K., et al. 2006, PASJ, this volume
Palmeri, P., Mendoza, C., Kallman, T. R., Bautista, M. A., & Meléndez, M. 2003, A&A, 410, 359
Petre, R., Allen, G. E., & Hwang, U., 1999, Astron. Nachr., 320, 199
Porquet, D., Arnaud, M., & Decourchelle, A. 2001, A&A, 373, 1110
Rho, J., Dyer, K. K., Borkowski, K. J., & Reynolds, S. P. 2002, ApJ, 581, 1116
Rosado, M., Ambrocio-Cruz, P., Le Coarer, E., & Marcelin, M. 1996, A&A, 315, 243
Serlemitsos, P., et al. 2006, PASJ, this volume
Slane, P., Hughes, J. P., Edgar, R. J., Plucinsky, P. P., Miyata, E., Tsunemi, H., & Aschenbach, B. 2001, ApJ, 548, 814
Takahashi, T., et al. 2006, PASJ, this volume
Valinia, A., Tatischeff, V., Arnaud, K., Ebisawa, K., & Ramaty, R. 2000, ApJ, 543, 733
Vink, J., Kaastra, J. S., & Bleeker, J. A. M. 1997, A&A, 328, 628
Vink, J., van der Heyden, K., Bleeker, J. A. M., Bykov, A., Bamba, A., Yamazaki, R. 2006, ApJaccepted, astro-ph 0607307